Working Notes on Glucose–Insulin Modeling

Based on the Dalla Man (2007) Meal Simulation Model

Krishna

January 4, 2026

Contents

1 Model Definition and Operating Regime

This section defines the dynamical model that serves as the common foundation for all subsequent diagnostic tests. The purpose here is not to re-derive or re-justify the physiological model in full generality, but to state precisely *which* equations are used, *how* they are implemented, *under what operating regime* they are simulated, and *what scope of validity* the resulting analyses are intended to have. All later results are conditional on the definitions and assumptions made explicit in this section.

1.1 Model Origin and Scope

The model employed in this work is a faithful implementation of the postprandial glucose–insulin simulation model introduced by Dalla Man, Rizza, and Cobelli (2007). That model was originally developed to describe glucose and insulin dynamics following a mixed meal in normal human subjects, using a subsystem-based forcing function strategy supported by extensive tracer data. The present implementation follows the same structural decomposition into glucose kinetics, insulin kinetics, gastric emptying, intestinal absorption, endogenous glucose production, insulin action, and insulin secretion.

The model is used here strictly as an *open-loop physiological system*. No feedback control laws, estimation algorithms, or adaptive mechanisms are embedded in the dynamics. Inputs represent external physiological stimuli (meal ingestion and insulin infusion), and outputs correspond to measurable concentrations. The model is interrogated as a nonlinear dynamical system whose internal structure is assumed known, but whose state relevance, time-scale structure, identifiability properties, and output sensitivity are not assumed *a priori*.

1.2 State Vector and Physical Interpretation

The system is represented by a twelve-dimensional state vector

$$x(t) = \begin{bmatrix} G_p & G_t & I_l & I_p & Q_{\text{sto1}} & Q_{\text{sto2}} & Q_{\text{gut}} & I_1 & I_d & X \\ I_{\text{po}} & Y & & & & & & & & \end{bmatrix}^\top,$$

where each component has a specific physiological interpretation:

G_p : plasma glucose mass,
G_t : glucose mass in rapidly equilibrating tissues,
I_l : insulin mass in the liver,
I_p : insulin mass in plasma,
Q_{sto1} : glucose mass in the solid stomach compartment,
Q_{sto2} : glucose mass in the triturated stomach compartment,
Q_{gut} : glucose mass in the intestine,
I_1 : remote insulin compartment (delay chain),
I_d : delayed insulin signal,
X : insulin action on glucose utilization,
I_{po} : portal insulin mass,
Y : auxiliary dynamic state linking glucose to insulin secretion.

All states are continuous and evolve according to coupled nonlinear ordinary differential equations. None of the internal states are assumed directly measurable except through their influence on the chosen output.

1.3 Governing Equations

The full model consists of the following components:

Glucose kinetics. Plasma and tissue glucose masses evolve according to

$$\dot{G}_p = \text{EGP} + R_a - E - U_{ii} - k_1 G_p + k_2 G_t, \tag{1}$$
$$\dot{G}_t = -U_{id} + k_1 G_p - k_2 G_t, \tag{2}$$

where EGP is endogenous glucose production, R_a is the rate of glucose appearance from the gut, U_{ii} is exogenous insulin infusion, U_{id} is insulin-dependent glucose utilization, and k_1, k_2 are inter-compartmental exchange rates.

Insulin kinetics. Liver and plasma insulin dynamics are given by

$$\dot{I}_l = -(m_1 + m_3) I_l + m_2 I_p + S, \tag{3}$$
$$\dot{I}_p = -(m_2 + m_4) I_p + m_1 I_l, \tag{4}$$

where S denotes insulin secretion and m_i are degradation and exchange parameters. Hepatic extraction is modeled as time-varying through its dependence on portal insulin.

Gastrointestinal absorption. Meal glucose transit is described by

$$\dot{Q}_{\text{sto1}} = -k_{\text{gri}} Q_{\text{sto1}}, \tag{5}$$
$$\dot{Q}_{\text{sto2}} = -k_{\text{empt}} Q_{\text{sto2}} + k_{\text{gri}} Q_{\text{sto1}}, \tag{6}$$
$$\dot{Q}_{\text{gut}} = -k_{\text{abs}} Q_{\text{gut}} + k_{\text{empt}} Q_{\text{sto2}}, \tag{7}$$

where k_{empt} is a nonlinear gastric emptying rate depending on stomach content, consistent with the original model formulation.

Insulin action and secretion. Insulin action and delayed signaling are captured by

$$\dot{I}_1 = -k_i(I_1 - I), \tag{8}$$
$$\dot{I}_d = -k_i(I_d - I_1), \tag{9}$$
$$\dot{X} = -p_{2U} X + p_{2U}(I - I_b), \tag{10}$$

while insulin secretion dynamics are governed by

$$\dot{I}_{\text{po}} = -\gamma I_{\text{po}} + S_{\text{po}}, \tag{11}$$
$$\dot{Y} = -\alpha(Y - \beta(G - G_b)), \tag{12}$$

with S_{po} representing glucose-dependent pancreatic secretion.

1.4 Inputs, Outputs, and Measurement Assumptions

Two external inputs are considered throughout this work:

- Exogenous insulin infusion $U_{ii}(t)$.
- Meal ingestion, represented as an initial gastric glucose load in Q_{sto1}.

No time-varying oral ingestion rate is used; instead, meal size is encoded through the initial condition of the gastric compartment.

The sole measured output considered in all diagnostic tests is *plasma glucose*,

$$y(t) = G_p(t).$$

All other states are treated as latent. This restriction is deliberate and reflects the practical limitation of glucose-centric measurement scenarios, such as those encountered in continuous glucose monitoring.

1.5 Operating Regime and Initial Conditions

All simulations are performed in a normoglycemic, non-pathological operating regime corresponding to a normal subject. Initial conditions represent a postprandial configuration with nonzero gastric glucose content and physiologically plausible basal glucose and insulin levels. The initial state is not assumed to be an exact steady state, and transient dynamics following meal ingestion are central to the analyses that follow.

1.6 Renal Glucose Excretion

In the original Dalla Man model, renal glucose excretion is active only when plasma glucose exceeds a threshold. In the present implementation, renal excretion is explicitly set to zero for all simulations. This choice reflects two considerations: first, the operating regime remains below the renal threshold throughout the experiments of interest; second, disabling this term avoids numerical pathologies without altering glucose dynamics in the normoglycemic range. Consequently, all conclusions drawn in this work are restricted to regimes where renal glucose excretion is physiologically inactive.

1.7 Scope and Regime of Validity

The analyses presented in this document are conditional on the following assumptions:

1. The model structure accurately represents postprandial glucose–insulin dynamics in normal subjects.
2. The system operates in a regime where renal glucose excretion is negligible.
3. Plasma glucose is the only available measurement.

No claims are made regarding hyperglycemic conditions, pathological insulin resistance, or closed-loop control performance. Within this scope, the model serves as a well-defined nonlinear dynamical system on which structural, dynamical, and identifiability diagnostics can be meaningfully applied.

2 Diagnostic Philosophy and Scope

The purpose of this section is to articulate the epistemic framework underlying the sequence of diagnostic tests performed in this study. Rather than introducing additional model equations or numerical results, the goal here is to clarify *why* multiple tests are required, *what type of information* each test is intended to extract from the nonlinear model, and *how outcomes such as degeneracy, rank deficiency, or weak sensitivities are to be interpreted*. This section establishes the rules of interpretation that govern all subsequent analyses.

2.1 Nature and Intent of the Document

This document is intentionally positioned at the intersection of three complementary roles: it functions simultaneously as a research notebook, a thesis-style technical report, and a precursor to a potential journal-level study. As such, the emphasis is on transparency of assumptions, explicit linkage between theory and numerical evidence, and careful delimitation of the scope of any conclusions drawn.

The analyses presented here are not designed to demonstrate model correctness in a predictive sense, nor to optimize performance metrics for control or estimation. Instead, the model is treated as a fixed nonlinear dynamical system whose internal structure is assumed known, and the objective is to interrogate that structure using multiple, conceptually distinct diagnostic lenses. The document therefore prioritizes interpretability and structural insight over compactness or presentation-driven simplification.

2.2 Why Multiple Diagnostic Tests Are Necessary

For nonlinear physiological systems of the complexity considered here, no single diagnostic tool can simultaneously answer questions of dynamical relevance, time-scale structure, identifiability, and output influence. Each of these properties addresses a different aspect of the relationship between internal states, external inputs, and measured outputs.

In particular, the following limitations motivate the use of multiple tests:

- A state may be dynamically active yet have negligible influence on the measured output.
- A state may strongly influence the output but remain weakly excited under admissible inputs.
- States may be distinguishable in principle but collapse onto low-dimensional manifolds along specific trajectories.
- Apparent non-identifiability may arise either from structural coupling or from insufficient excitation.

Because these failure modes are logically distinct, they cannot be ruled out by a single analysis. The four diagnostic tests employed in this work are therefore designed to probe orthogonal structural properties of the same underlying model. Strong conclusions are drawn only where results are consistent across tests; disagreements are treated as informative rather than problematic.

2.3 Interpretation of Failures and Degeneracies

A central interpretive principle adopted throughout this document is that numerical or statistical pathologies are treated as *results*, not errors. In particular, the following outcomes are explicitly not regarded as implementation failures:

- Low-rank or ill-conditioned Fisher information matrices,
- Flat or weakly curved likelihood profiles,
- Near-zero empirical energies or sensitivities,
- Strong clustering of time scales or apparent slaving of states.

When such phenomena arise, they are interpreted as manifestations of the model's internal structure, the chosen operating regime, or the informational content of the applied inputs and outputs. Only clear numerical instabilities or violations of stated assumptions are considered implementation issues. This distinction is critical for avoiding over-interpretation of numerical success and under-interpretation of numerical failure.

2.4 Best-Case Versus Realistic Assumptions

Several methodological choices made in later sections, such as the use of rich excitation signals, long simulation horizons, or simplified noise models, are intentionally biased toward *best-case* conditions. These choices are not intended to reflect realistic operational scenarios, but rather to test the intrinsic structural limits of the model.

In particular, when optimistic assumptions fail to yield identifiability, separation, or dominance, this failure is taken as strong evidence that the corresponding property is unlikely to hold under more realistic conditions. Conversely, success under best-case assumptions is interpreted cautiously and does not imply robustness outside the tested regime.

2.5 Independence and Ordering of Diagnostic Tests

Each diagnostic test introduced in this document is designed to address a distinct question:

1. Empirical input–output energy analysis probes which states are dynamically activated by admissible inputs and reflected in the output.
2. Time-scale separation analysis examines whether the dynamics exhibit fast–slow structure or low-dimensional attracting manifolds along observed trajectories.
3. Excitation-rich identifiability analysis investigates whether structural distinguishability can be recovered under deliberately informative inputs.
4. Output map sensitivity analysis isolates which states directly shape the measured glucose dynamics over time.

The ordering of these tests is deliberate. Earlier tests focus on dynamical relevance and structure, while later tests address identifiability and measurement influence. No test is claimed to be sufficient on its own; rather, the collective pattern of results across tests forms the basis for subsequent synthesis and interpretation.

2.6 Scope of Claims

All conclusions drawn in later sections are conditional on the diagnostic philosophy articulated here. Specifically, claims are limited to:

- The operating regimes and inputs explicitly tested,
- The choice of plasma glucose as the sole measured output,
- The interpretation of results under best-case excitation assumptions.

Within this scope, the diagnostic framework provides a structured and defensible basis for assessing model structure, reduced-order modeling potential, and estimation limitations. Beyond this scope, no extrapolations are implied.

3 Test I: Empirical Input–Output Energy Analysis

This section introduces the first diagnostic test applied to the nonlinear glucose–insulin model: an empirical input–output energy analysis. The purpose of this test is to identify which internal states actively participate in the transmission of physiologically admissible inputs to the measured output, without invoking linearization, stochastic assumptions, or parameter estimation. This test is deliberately positioned as the initial diagnostic because it relies on minimal structural assumptions and probes the realized nonlinear dynamics directly.

3.1 Motivation and Conceptual Basis

In high-dimensional nonlinear physiological models, the mere presence of a state variable does not imply dynamical relevance for a given operating regime. A state may be structurally coupled to others yet remain dynamically dormant, weakly excited, or effectively invisible at the output under admissible inputs. Conversely, a state may dominate system behavior only transiently or only through indirect pathways.

Classical controllability and observability concepts, defined via Gramians, are not directly applicable here because the system is nonlinear, time-varying along trajectories, and not analyzed around a fixed equilibrium. Rather than attempting to generalize these concepts analytically, this test adopts an empirical perspective: state relevance is assessed by measuring how strongly each state is excited by input perturbations and how strongly that excitation co-varies with the measured output along the resulting nonlinear trajectories.

The guiding question of this test is therefore:

> Which states of the nonlinear model carry significant input–output energy under physiologically meaningful perturbations?

3.2 Empirical Energy Definitions

Let $x_i(t)$ denote the i-th state trajectory of the nonlinear system resulting from a prescribed input experiment, and let $y(t) = G_p(t)$ denote the measured plasma glucose output. Two empirical energy measures are defined.

First, an empirical controllability energy is associated with each state,

$$W_{c,i} = \int_0^T x_i(t)^2 \, \mathrm{d}t, \tag{13}$$

which quantifies the total activation of state i over the observation horizon T in response to external inputs. This quantity does not represent reachability in a formal sense; rather, it measures realized state excitation along the chosen trajectories.

Second, an empirical observability energy is defined as

$$W_{o,i} = \int_0^T \left(x_i(t)\, y(t)\right)^2 \, \mathrm{d}t, \tag{14}$$

which quantifies the extent to which variations in state i are reflected in the output over time. States whose trajectories remain weakly correlated with the output yield negligible observability energy, even if they are dynamically active.

To combine these two aspects, a joint state influence metric is constructed as

$$I_i = \sqrt{W_{c,i}\, W_{o,i}}, \tag{15}$$

which mirrors, in an empirical nonlinear setting, the role played by Hankel singular values in linear balanced truncation. The influence values are subsequently normalized by the maximum across all states,

$$\tilde{I}_i = \frac{I_i}{\max_j I_j}, \tag{16}$$

so that state importance is assessed on a relative scale.

3.3 Input Design and Experimental Protocol

The empirical energies are computed by subjecting the model to two independent, physiologically interpretable input experiments. These experiments are designed to excite distinct subsystems of the model without introducing artificial or non-physiological forcing.

Insulin impulse experiment. An insulin infusion perturbation is applied by temporarily increasing the exogenous insulin input $U_{ii}(t)$ over a short time window. Outside this window, the infusion remains at its nominal basal value. This experiment preferentially excites insulin kinetics, insulin action pathways, and their downstream effects on glucose dynamics.

Meal-related perturbation. A second experiment perturbs the gastrointestinal subsystem by introducing a transient increase in the effective meal-related parameter governing gastric emptying and absorption. Although the base meal is encoded through initial conditions, this perturbation acts as a localized excitation of the gastric and intestinal compartments, thereby probing the sensitivity of downstream glucose appearance.

Both experiments are applied independently, starting from the same initial condition and parameter set, and the resulting state trajectories are simulated over a fixed observation horizon. The empirical controllability energy is computed by summing contributions from both experiments, ensuring that states relevant to either insulin-driven or meal-driven dynamics are captured.

3.4 Problem Formulation for the Dalla Man Model

Let $x(t; u^{(k)})$ denote the state trajectory resulting from the k-th input experiment, with $k \in \{\text{insulin}, \text{meal}\}$. The empirical controllability energy is computed as

$$W_{c,i} = \sum_k \int_0^T x_i(t; u^{(k)})^2 \, \mathrm{d}t, \tag{17}$$

while the empirical observability energy is computed using the insulin-perturbed trajectory,

$$W_{o,i} = \int_0^T \left(x_i(t; u^{(\text{insulin})}) \, G_p(t; u^{(\text{insulin})}) \right)^2 \mathrm{d}t. \tag{18}$$

The choice to evaluate observability with respect to plasma glucose reflects the measurement constraint imposed throughout this document. No assumptions are made regarding noise, linearity, or stationarity. All energies are trajectory-dependent and conditioned on the chosen input ensemble.

3.5 Interpretational Limits of the Test

It is essential to emphasize what this test does and does not establish. A high empirical influence indicates that a state is dynamically active and contributes to the measured output under the specific input experiments considered. A low influence does not imply that the state is unimportant in a structural or physiological sense; rather, it indicates that the state is effectively dormant, slaved, or weakly coupled in the tested operating regime.

Accordingly, this test provides a *necessary but not sufficient* condition for state relevance in reduced-order modeling and estimation. States identified as influential here are candidates for retention, while states with negligible influence require further scrutiny through additional diagnostics before any truncation decisions are made.

The numerical results of this test, including state rankings and their implications, are presented and interpreted in the following section.

4 Results of Test I: Empirical Input–Output Energy Ranking

This section reports the numerical outcomes of the empirical input–output energy analysis described in the previous section. The results are presented as a ranked state influence profile and interpreted strictly within the scope of this diagnostic test, without invoking conclusions from subsequent analyses.

4.1 Observed State Influence Distribution

Figure 1 shows the normalized empirical joint influence values for all twelve states of the model, ordered from highest to lowest influence. The influence values are normalized by the maximum across states, so that the ranking reflects relative, not absolute, importance.

A strikingly sparse influence structure is observed. Only three states exhibit non-negligible influence:

$$\begin{aligned} Q_{\mathrm{sto2}} &: \text{ triturated stomach compartment,} \\ Q_{\mathrm{sto1}} &: \text{ solid stomach compartment,} \\ Q_{\mathrm{gut}} &: \text{ intestinal glucose compartment.} \end{aligned}$$

Among these, the triturated stomach compartment Q_{sto2} dominates by a wide margin. The solid stomach compartment Q_{sto1} contributes at a substantially lower level, followed by the intestinal compartment Q_{gut}. All remaining states exhibit influence values several orders of magnitude smaller, effectively collapsing to zero on the normalized scale.

4.2 Dominance of Gastrointestinal States

The dominance of the gastrointestinal compartments is a direct consequence of the input design and output choice. Both applied perturbations—the insulin impulse and the meal-related perturbation—ultimately affect plasma glucose through the pathway of glucose appearance. As a result, states governing gastric emptying and intestinal absorption accumulate substantial empirical controllability energy. Because fluctuations in these states directly modulate the glucose appearance term R_a, they also exhibit strong empirical observability with respect to plasma glucose.

In contrast, downstream states such as plasma glucose G_p, tissue glucose G_t, insulin masses, and insulin action variables appear weakly influential under this metric. Their trajectories are largely shaped by the upstream gastrointestinal dynamics and exhibit limited independent variation relative to the output when integrated over the full postprandial horizon.

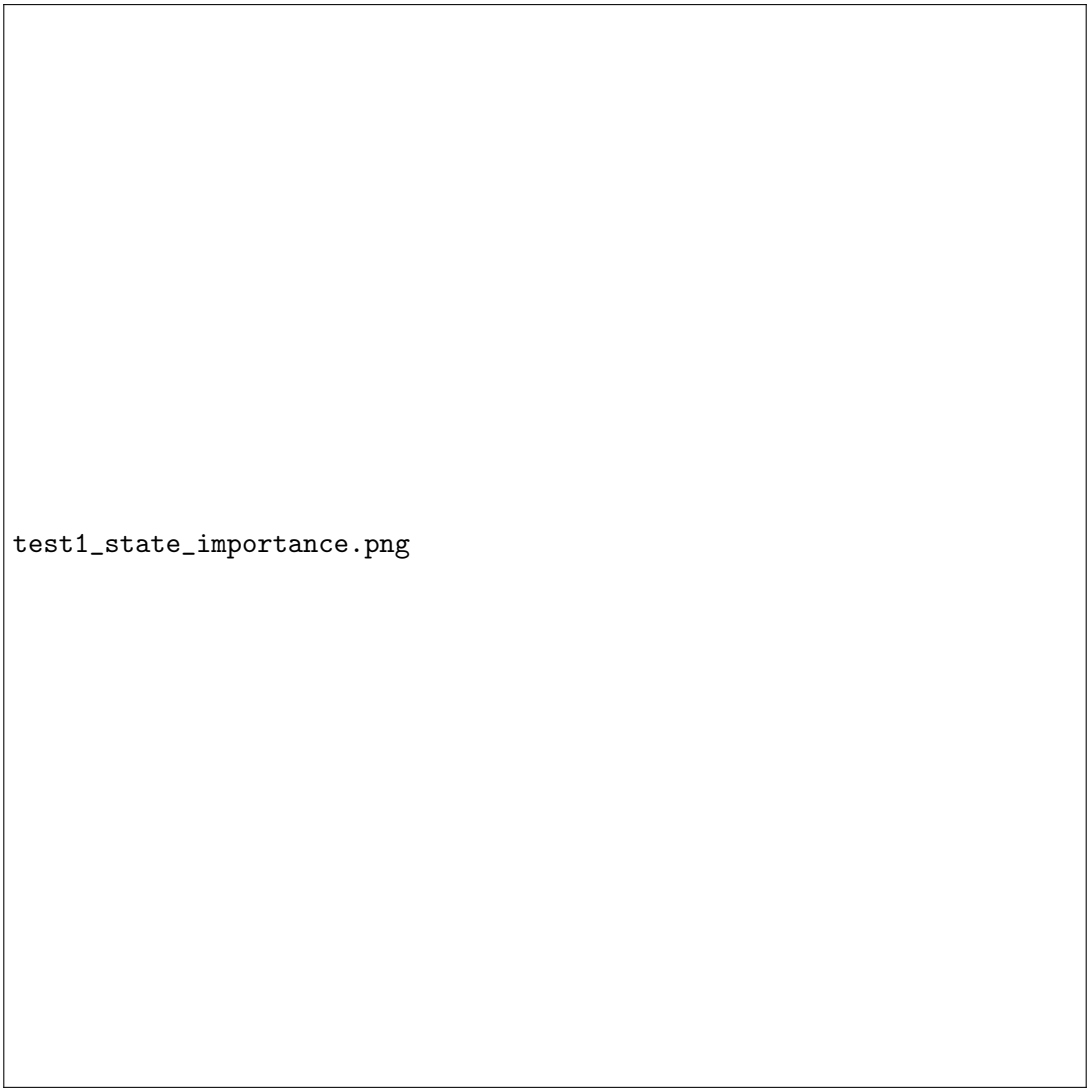

Figure 1: Normalized empirical input–output energy for each state of the nonlinear glucose–insulin model. Influence values are computed as the geometric mean of empirical controllability and observability energies and normalized by the maximum across states. States are ordered from highest to lowest influence.

4.3 Interpretation of Near-Zero Influence Values

States with near-zero empirical influence are not interpreted as physiologically irrelevant. Rather, these results indicate that, under the tested operating regime and input ensemble, such states are dynamically slaved, weakly excited, or redundant with respect to the measured output. In particular, insulin-related states may remain essential for internal regulation while contributing little incremental information to the plasma glucose signal under the specific perturbations applied.

The extreme separation between the dominant and non-dominant states also reflects the trajectory-integrated nature of the energy metric. States that influence glucose only transiently or indirectly may fail to accumulate sufficient joint energy to appear influential in this ranking.

4.4 Implications and Limitations of Test I

The empirical input–output energy analysis reveals that, for the chosen inputs and normoglycemic regime, the effective dimensionality of the input–output dynamics is extremely low and dominated by the gastrointestinal subsystem. This finding provides an initial indication that substantial state redundancy may be present from the perspective of reduced-order modeling.

However, this test alone does not establish whether low-influence states can be safely removed from a reduced model, nor whether the observed dominance persists under different excitation conditions or time windows. The results of Test I therefore serve as a preliminary screening step, motivating further diagnostics aimed at time-scale structure, identifiability, and output sensitivity, which are addressed in the subsequent sections.

5 Test II: Time-Scale Separation Analysis

This section formulates the second diagnostic test, which examines the presence and structure of time-scale separation in the nonlinear glucose–insulin model. The analysis is entirely trajectory-based and is designed to expose fast–slow structure, stiffness, and state slaving by probing the local linear relaxation properties of the nonlinear dynamics along physiologically meaningful operating points. No reduced-order approximation or truncation is performed in this test.

5.1 Motivation

In nonlinear physiological systems, large disparities in intrinsic time scales are common and often arise from the coupling of fast biochemical processes with slower transport, storage, or regulatory mechanisms. Such disparities can lead to stiff dynamics, low-dimensional attracting manifolds, and effective slaving of certain states to others. Identifying these features is essential for understanding which dynamical degrees of freedom evolve independently and which are constrained by faster processes.

Unlike the empirical energy analysis of Test I, which quantifies realized state participation under specific inputs, the present test interrogates the *local dynamical structure* of the system itself. The objective is to determine whether the nonlinear model exhibits well-separated relaxation modes and whether these modes persist across distinct phases of the postprandial response.

5.2 Trajectory-Based Local Linearization

Let the nonlinear system be written as

$$\dot{x}(t) = f(x(t), p),$$

where $x(t) \in \mathbb{R}^{12}$ is the state vector and p denotes the fixed parameter set. A baseline trajectory $x(t)$ is generated by simulating the open-loop system from the prescribed initial condition with no additional perturbations beyond those encoded in the initial state.

At selected time instants $t = t^*$ along this trajectory, the system is locally linearized via the

Jacobian matrix

$$J(x(t^*)) = \left.\frac{\partial f}{\partial x}\right|_{x=x(t^*)}.$$

Because closed-form expressions for the Jacobian are not used, the partial derivatives are approximated numerically using forward finite differences applied to the full nonlinear vector field. This construction preserves the full nonlinear structure of the model while providing a local linear diagnostic of the dynamics.

5.3 Eigenvalue Analysis and Time-Scale Definition

For each selected operating point, the eigenvalue problem

$$J(x(t^*))v = \lambda v$$

is solved. Only eigenvalues with strictly negative real parts are retained, corresponding to locally stable relaxation modes of the dynamics.

Each retained eigenvalue λ_i is associated with a local linear time constant defined as

$$\tau_i = -\frac{1}{\Re(\lambda_i)}.$$

These time constants quantify the rate at which small perturbations along the corresponding eigendirections decay back toward the trajectory. No assumptions are made regarding modal dominance or global validity; the quantities are interpreted strictly as local relaxation measures.

5.4 Selection of Operating Points

The time-scale analysis is performed at a small number of physiologically meaningful points along the baseline trajectory. These points are selected to represent qualitatively distinct phases of the postprandial response:

- an early postprandial phase shortly after meal ingestion,
- the time of peak plasma glucose concentration,
- a late recovery phase following glucose clearance.

At each of these operating points, the Jacobian spectrum and associated time constants are computed independently. This allows assessment of whether time-scale separation is transient or persists across the trajectory.

5.5 Assessment of Time-Scale Separation

For each operating point, the fastest and slowest local time constants are identified, and their ratio is used as a quantitative measure of separation. In addition to pointwise analysis, all time constants obtained across operating points are aggregated and examined on a logarithmic scale to reveal clustering and spectral gaps.

A pronounced gap in the distribution of $\log_{10}(\tau)$ values is interpreted as evidence of a natural division between fast and slow dynamical modes. This interpretation is purely diagnostic: no reduction or projection onto slow manifolds is performed at this stage.

5.6 State-Wise Characteristic Time Scales

Beyond modal time constants, a state-centric characterization of time scales is constructed. At a representative operating point, the eigenvectors of the Jacobian are used to compute a participation measure for each state in each eigenmode. For a given state, the contributions of all stable modes are combined using a weighted geometric mean of their associated time constants. The resulting quantity provides a single characteristic relaxation time for each state, summarizing how that state participates across fast and slow modes.

This construction does not imply that a state evolves on a single time scale; rather, it provides a compact descriptor of the dominant relaxation behavior associated with that state under local linear dynamics.

5.7 Interpretational Scope

This test is intended to diagnose the presence of fast–slow structure and stiffness in the nonlinear model. It does not establish global invariance of time scales, does not justify state truncation by itself, and does not account for nonlinear transient amplification or input-dependent effects. The results of this test are therefore interpreted as complementary to, rather than substitutive of, the other diagnostics presented in this document.

Numerical results, eigenvalue spectra, and time-scale distributions arising from this analysis are presented in the following section.

6 Results of Test II: Time-Scale Separation Analysis

This section presents the numerical outcomes of the trajectory-based time-scale separation analysis introduced in the previous section. The results are derived directly from the local Jacobian eigenstructure of the nonlinear model evaluated along a baseline postprandial trajectory. All reported quantities follow exactly from the implemented computations and are interpreted strictly within the scope of this diagnostic.

6.1 Eigenvalue Structure at Representative Operating Points

The local Jacobian spectra were evaluated at three physiologically meaningful points along the postprandial trajectory: an early postprandial phase, the time of peak plasma glucose, and a late recovery phase. At each operating point, the eigenvalues of the Jacobian exhibit a consistent qualitative structure.

In all cases, the spectrum is confined to the left half of the complex plane, indicating locally stable dynamics around the trajectory. The real parts of the eigenvalues span more than two orders of magnitude, with a small number of modes clustered close to the imaginary axis and several modes located far into the negative real region. Complex conjugate pairs are present, but their imaginary parts remain small relative to the spread in real parts, indicating weakly oscillatory behavior superimposed on predominantly relaxational dynamics.

The qualitative similarity of the eigenvalue distributions across early postprandial, peak, and recovery phases indicates that the local linear structure of the dynamics is preserved throughout the trajectory, despite substantial changes in the state values themselves.

6.2 Local Time Constants and Separation Ratios

For each operating point, local linear time constants were computed from the real parts of the stable eigenvalues. Across all three phases, the fastest time constants are on the order of one minute, while the slowest time constants are on the order of one to two hours. The resulting separation ratios between the slowest and fastest modes are consistently on the order of 10^2.

The persistence of this large separation ratio across all sampled operating points provides strong evidence that the model exhibits pronounced multi-time-scale structure. Importantly, this separation is not confined to a specific transient phase but is present during early response, peak glucose, and recovery dynamics alike.

6.3 Distribution of Time Scales

Aggregating all computed time constants across operating points and examining their distribution on a logarithmic scale reveals a clear clustering pattern. The histogram of $\log_{10}(\tau)$ values exhibits distinct groups corresponding to fast and slow modes, separated by a noticeable gap.

This gap suggests the presence of a natural division between fast-relaxing and slow-relaxing dynamical components. The identification of such a spectral gap is consistent with the notion of stiffness and supports the interpretation that certain modes rapidly equilibrate relative to the dominant slow dynamics governing postprandial glucose evolution.

The detection of this gap is purely diagnostic. No projection, truncation, or explicit fast–slow decomposition is performed on the system at this stage.

6.4 State-Wise Characteristic Time Scales

In addition to modal time constants, characteristic time scales were computed for each state using eigenvector participation weights derived from the local Jacobian at the initial operating point. This construction assigns each state a single representative relaxation time reflecting its weighted participation across all stable modes.

The resulting state-wise time scales span a wide range, mirroring the modal separation observed in the eigenvalue analysis. Some states are dominated by fast modes and exhibit short characteristic time constants, while others are associated primarily with slow modes and evolve on substantially longer time horizons. This heterogeneity indicates that, even though all states are dynamically coupled, they do not contribute equally to fast and slow processes.

These characteristic time scales are not interpreted as exact physical relaxation times for individual states. Rather, they provide a compact summary of how each state participates in the multi-time-scale structure of the local linearized dynamics.

6.5 Interpretation and Limitations

The results of Test II demonstrate that the nonlinear glucose–insulin model exhibits strong and persistent time-scale separation along a physiologically relevant trajectory. The presence of large separation ratios and a clear spectral gap indicates stiffness and suggests the existence of slaving relationships, whereby fast modes rapidly adjust to constrain the evolution of slower dynamics.

However, these findings are strictly local and diagnostic. They do not imply global invariance of time scales, nor do they justify state truncation or reduced-order modeling decisions in

isolation. The analysis does not account for nonlinear transient amplification, input-dependent effects, or changes in stability under alternative excitation conditions.

Accordingly, the time-scale separation identified here is treated as structural evidence of fast–slow organization in the dynamics, to be integrated with the outcomes of subsequent diagnostics addressing identifiability and output sensitivity.

7 Test III: Excitation-Rich Identifiability Analysis

This section formulates the third diagnostic test, which examines the practical identifiability of selected model parameters under deliberately excitation-rich experimental conditions. Unlike the previous tests, which focused on dynamical relevance and time-scale structure, the present analysis directly addresses the question of whether parameter values can, even in principle, be inferred from measurements of plasma glucose alone when the system is driven by highly informative inputs.

The formulation of this test is strictly grounded in the implemented code and numerical procedures. No assumptions beyond those explicitly encoded are introduced, and the analysis is intentionally framed as a best-case diagnostic.

7.1 Motivation

In nonlinear physiological models, lack of identifiability may arise from two fundamentally different sources. The first is insufficient excitation: parameters may be theoretically distinguishable, but the applied inputs fail to sufficiently perturb the relevant pathways. The second is structural non-identifiability: parameters may be intrinsically confounded due to the algebraic and dynamical structure of the model, rendering them indistinguishable regardless of excitation richness.

Test III is designed to discriminate between these two possibilities. By constructing an experiment that maximizes temporal richness and diversity of excitation within physiologically admissible bounds, the test probes whether poor identifiability observed under standard conditions can be alleviated by improved experimental design. Failure to improve identifiability under such conditions is interpreted as strong evidence of structural limitations.

7.2 Parameters and Output Considered

The analysis focuses on a selected subset of physiologically meaningful parameters governing glucose kinetics and insulin action. Identifiability is assessed exclusively with respect to the plasma glucose concentration $G_p(t)$, which is treated as the sole measured output throughout this document.

No auxiliary measurements, latent states, or synthetic outputs are introduced. All conclusions are therefore conditional on the restriction to glucose-only observation.

7.3 Excitation Design

Two distinct experimental conditions are considered.

Standard experiment. The standard experiment corresponds to a baseline postprandial simulation with nominal insulin infusion and a single meal input. No additional perturbations are applied beyond those inherent to the initial condition and baseline inputs.

Designed excitation-rich experiment. The designed experiment introduces deliberate temporal richness into the inputs while preserving physiological plausibility. This includes multiple, time-localized perturbations in insulin infusion and a temporally distributed meal input. The perturbations are bounded in magnitude and duration and are chosen to excite multiple pathways and time scales of the model.

The designed experiment is not intended to represent a realistic clinical protocol. Rather, it serves as an optimistic, information-maximizing scenario against which structural identifiability can be tested.

7.4 Sensitivity Computation

Parameter sensitivities are computed empirically using finite differences. For each parameter p_i, a perturbed simulation is generated with a small relative change in the parameter value, while all other parameters are held fixed. The resulting output sensitivity is approximated as

$$S_i(t) = \frac{G_p(t; p_i(1+\varepsilon)) - G_p(t; p_i)}{\varepsilon\, p_i},$$

with a fixed relative perturbation magnitude ε.

To ensure scale consistency across parameters and time, sensitivities are normalized by a characteristic scale derived from the glucose output. This normalization renders the subsequent information measures dimensionless and prevents dominance by parameters with purely numerical scaling advantages.

7.5 Fisher Information Matrix Construction

The Fisher Information Matrix (FIM) is constructed empirically from the time-discretized sensitivity matrix. Let $S \in \mathbb{R}^{N\times m}$ denote the sensitivity matrix formed by stacking the sensitivities of the output with respect to the m parameters over N time points. The FIM is defined as

$$F = \frac{1}{N} S^\top S.$$

No explicit noise covariance is introduced; this corresponds to an implicit assumption of homoscedastic, uncorrelated measurement noise. This choice is deliberately optimistic and serves to test identifiability under favorable conditions. Eigenvalues of the FIM are computed to assess parameter distinguishability, and a condition number is formed from the ratio of the largest to the smallest retained eigenvalue.

7.6 Interpretational Scope

This test assesses practical parameter identifiability under excitation-rich conditions using an empirical Fisher Information framework. It does not claim global identifiability, does not address estimator performance, and does not incorporate realistic measurement noise models. An

improvement in conditioning under designed excitation would suggest excitation-limited identifiability, whereas persistence or worsening of ill-conditioning under richer excitation is interpreted as evidence of structural non-identifiability.

Numerical results, eigenvalue spectra, and their implications are presented in the following section.

8 Results of Test III: Excitation-Rich Identifiability Analysis

This section presents the numerical outcomes of the excitation-rich identifiability analysis formulated in the previous section. The results are derived directly from the implemented sensitivity calculations, Fisher Information Matrix (FIM) construction, and eigenvalue analysis, and are interpreted strictly within the scope of glucose-only observation.

8.1 Glucose Response Under Standard and Designed Excitation

Figure 2 compares the plasma glucose trajectories generated under the standard and designed excitation conditions. The designed experiment produces markedly richer temporal structure in the glucose response, including sharper transients, additional inflection points, and altered recovery dynamics relative to the standard experiment.

This qualitative change in the output trajectory confirms that the designed excitation successfully perturbs the system across multiple time windows and operating regimes. Consequently, any failure to improve identifiability cannot be attributed to a lack of excitation richness at the output level.

8.2 Sensitivity Structure and Parameter Excitation

Figure 3 illustrates the time-varying sensitivity of plasma glucose with respect to a representative parameter governing glucose distribution volume. Under the standard experiment, the sensitivity remains small in magnitude and slowly varying. In contrast, the designed experiment induces large-amplitude, time-localized sensitivity peaks aligned with periods of strong input perturbation.

This result demonstrates that the excitation-rich input significantly amplifies parameter sensitivities and distributes informative content across the time horizon. From a purely excitation-based perspective, the designed experiment is therefore strictly superior to the standard experiment.

8.3 Fisher Information Eigenvalue Spectra

Despite the increased excitation and sensitivity magnitude, the eigenvalue spectra of the Fisher Information Matrix reveal a contrasting outcome. Figure 4 shows the ordered FIM eigenvalues for both experimental conditions on a logarithmic scale.

While the largest eigenvalues increase substantially under the designed experiment, the smallest eigenvalues decrease further, resulting in a more extreme spread of information across parameter directions. Quantitatively, the condition number of the FIM increases from approximately 7.8×10^5 under the standard experiment to approximately 5.6×10^{10} under the designed experiment.

Figure 2: Plasma glucose trajectories under the standard experiment and the excitation-rich designed experiment. The designed input induces stronger temporal variability and multiple transients, indicating substantially richer excitation of the glucose dynamics.

8.4 Conditioning and Structural Implications

The dramatic deterioration of the FIM condition number under richer excitation constitutes the central result of Test III. Because the designed experiment demonstrably increases output variability and parameter sensitivities, the observed worsening of conditioning cannot be attributed to insufficient excitation or poor experimental design.

Instead, the results indicate that additional excitation preferentially amplifies already-informative parameter combinations while leaving weakly identifiable directions effectively unobservable. The increased separation between dominant and near-null eigenvalues exposes latent degeneracies in the parameter-to-output map, revealing that the loss of identifiability is structural rather than excitation-limited.

8.5 Interpretation and Limitations

The results of Test III provide strong evidence that the considered parameter subset is not practically identifiable from plasma glucose measurements alone, even under optimistic excitation-rich

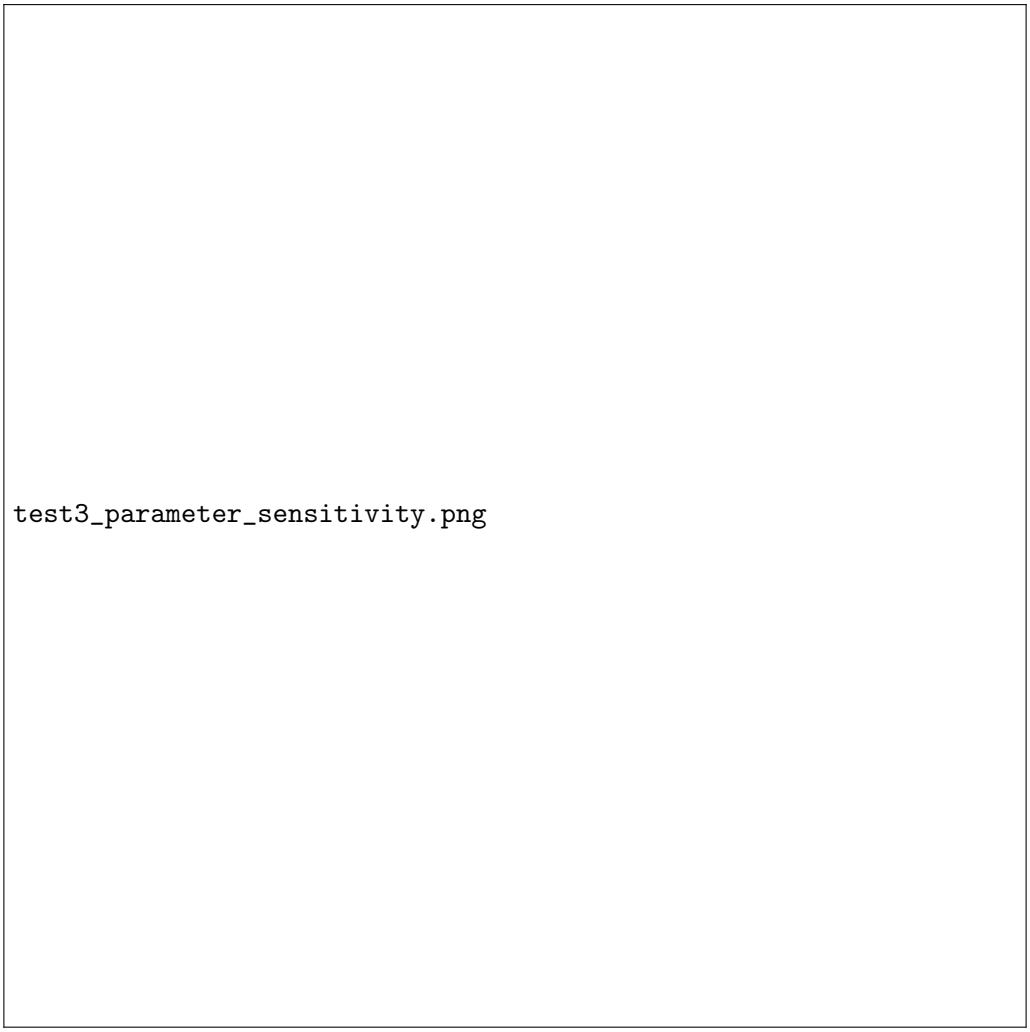

Figure 3: Time-varying sensitivity of plasma glucose with respect to a representative parameter under standard and designed excitation. The designed experiment produces larger and more structured sensitivities, confirming effective parameter excitation.

conditions. The failure of designed excitation to improve, and in fact its tendency to worsen, the conditioning of the Fisher Information Matrix indicates intrinsic confounding among parameters induced by the model structure and output restriction.

These conclusions are conditional on the use of plasma glucose as the sole measured output and on the optimistic assumptions implicit in the empirical FIM construction. No claims are made regarding identifiability under alternative measurement sets or with additional sensors. The findings of this test therefore motivate subsequent analysis of output sensitivity structure, addressed in the next diagnostic.

9 Test IV: Output Map Sensitivity Analysis

This section formulates the fourth diagnostic test, which examines how individual state variables influence the instantaneous dynamics of the measured output. Unlike the previous tests, which focused on energy transmission, time-scale structure, and parameter identifiability, the present analysis directly interrogates the local structure of the output map itself. The objective is to

Figure 4: Eigenvalue spectra of the Fisher Information Matrix under standard and excitation-rich designed experiments. Although excitation increases the dominant eigenvalues, the smallest eigenvalues collapse further, leading to worsened conditioning.

identify which states directly shape the evolution of plasma glucose and which states affect it only indirectly or negligibly.

9.1 Motivation

Reduced-order modeling and state elimination decisions depend not only on internal dynamics or identifiability considerations, but also on how state variables enter the output equation. A state may be dynamically active or strongly coupled internally while contributing little to the output dynamics of interest. Conversely, a state that appears weak in internal energy metrics may exert a direct and dominant influence on the output through algebraic or differential coupling.

Test IV is designed to isolate this distinction by analyzing the sensitivity of the glucose dynamics themselves, rather than the glucose trajectory. Specifically, the test examines how perturbations in each state affect the instantaneous rate of change of plasma glucose. This perspective allows direct identification of states that are structurally embedded in the output map.

9.2 Baseline Trajectory

The analysis is performed along a baseline postprandial trajectory generated by simulating the full nonlinear model under nominal conditions. No additional excitation or perturbation is applied beyond the baseline inputs encoded in the model configuration. This choice ensures that the output sensitivity structure reflects the natural operating regime of interest rather than artificially induced dynamics.

Let the nonlinear system be written as

$$\dot{x}(t) = f(x(t), p),$$

and let the plasma glucose state be denoted by $G_p(t)$. The baseline trajectory $x(t)$ is used as the reference around which local sensitivities are computed.

9.3 Definition of Output Map Sensitivity

Rather than analyzing the sensitivity of the glucose concentration itself, this test focuses on the sensitivity of its time derivative. At a given time t, the instantaneous glucose dynamics are given by

$$\dot{G}_p(t) = f_{G_p}(x(t), p),$$

where f_{G_p} denotes the component of the vector field corresponding to plasma glucose.

For each state x_i, the local sensitivity of the glucose dynamics is defined as

$$S_i(t) = \frac{\partial \dot{G}_p(t)}{\partial x_i}.$$

Because analytic expressions for these partial derivatives are not used, sensitivities are computed numerically via finite differences by perturbing one state at a time while holding all other states fixed.

9.4 Sampling Strategy and Aggregation

Sensitivities are evaluated at a finite number of time points uniformly sampled along the baseline trajectory. At each sampled time, the full state vector is perturbed sequentially, and the resulting change in $\dot{G}_p$ is recorded.

To summarize the influence of each state over the entire trajectory, the absolute sensitivities are aggregated using the mean over time,

$$\bar{S}_i = \frac{1}{N} \sum_{k=1}^{N} \left| S_i(t_k) \right|,$$

where $\{t_k\}$ denotes the sampled time points. This aggregation yields a single scalar measure of average influence for each state, reflecting its typical contribution to glucose dynamics rather than isolated transient effects.

For comparative purposes, the mean sensitivities are normalized by the maximum across all states, producing a relative influence scale.

9.5 Ranking and Thresholding

States are ranked in descending order of their normalized mean sensitivity. In addition, a threshold criterion is introduced to identify states with negligible influence on glucose dynamics. States whose mean sensitivity falls below a fixed fraction of the maximum are classified as low-influence states.

This threshold is not interpreted as a hard elimination rule, but rather as a diagnostic indicator highlighting states whose contribution to the output dynamics is minimal under the tested operating regime.

9.6 Direct versus Indirect Influence

Based on their role in the model structure, states are categorized as exerting either direct or indirect influence on glucose dynamics. States that appear explicitly in the glucose balance equation or its immediate coupling terms are labeled as direct, while states that affect glucose only through intermediate pathways are labeled as indirect.

This distinction is used solely for interpretive clarity and does not alter the numerical computation of sensitivities.

9.7 Interpretational Scope

Test IV characterizes the local structure of the output map along a nominal trajectory. It does not account for parameter uncertainty, alternative operating regimes, or nonlinear effects far from the baseline trajectory. The results are therefore conditional on the tested regime and on the restriction to plasma glucose as the sole output.

Nevertheless, by directly probing the sensitivity of the glucose dynamics themselves, this test provides complementary information to the preceding diagnostics and plays a central role in assessing which states are essential for accurately reproducing glucose behavior in reduced-order representations.

The numerical results and their implications are presented in the following section.

10 Results of Test IV: Output Map Sensitivity

This section presents the numerical results of the output map sensitivity analysis formulated in the previous section. The results quantify how individual state variables influence the instantaneous plasma glucose dynamics along a nominal postprandial trajectory. All conclusions are drawn directly from the computed sensitivities of $\dot{G}_p$ and are interpreted within the limits of this local, trajectory-based diagnostic.

10.1 Average State Influence on Glucose Dynamics

Figure 5 reports the normalized mean absolute sensitivity of the glucose dynamics $\dot{G}_p$ with respect to each state. The sensitivities are averaged over time and normalized by the maximum across states, yielding a relative influence scale.

A highly sparse influence structure is observed. Two states dominate the output map:

$$G_t \quad \text{and} \quad G_p,$$

Figure 5: Normalized mean absolute sensitivity of the glucose dynamics $\dot{G}_p$ with respect to each state, averaged along the baseline postprandial trajectory. The dashed line indicates a 1% relative influence threshold.

both of which enter directly into the glucose balance equations. A secondary tier of influence is associated with the portal insulin state I_{po}, followed by the delayed insulin signal I_d. All remaining states exhibit sensitivities that are several orders of magnitude smaller and collapse toward zero on the normalized scale.

10.2 Time-Varying Sensitivity of Dominant States

The temporal structure of output sensitivity for the most influential states is shown in Figure 6. The sensitivities of G_t and G_p remain approximately constant over the entire simulation horizon, reflecting their persistent and direct role in shaping glucose dynamics. In contrast, insulin-related states exhibit smaller magnitudes and limited temporal variation, indicating indirect modulation rather than direct control of $\dot{G}_p$.

The absence of sharp transients or phase-dependent sensitivity reversals suggests that the dominance hierarchy observed in the averaged sensitivities is not an artifact of temporal averaging, but reflects a stable structural property of the output map along the trajectory.

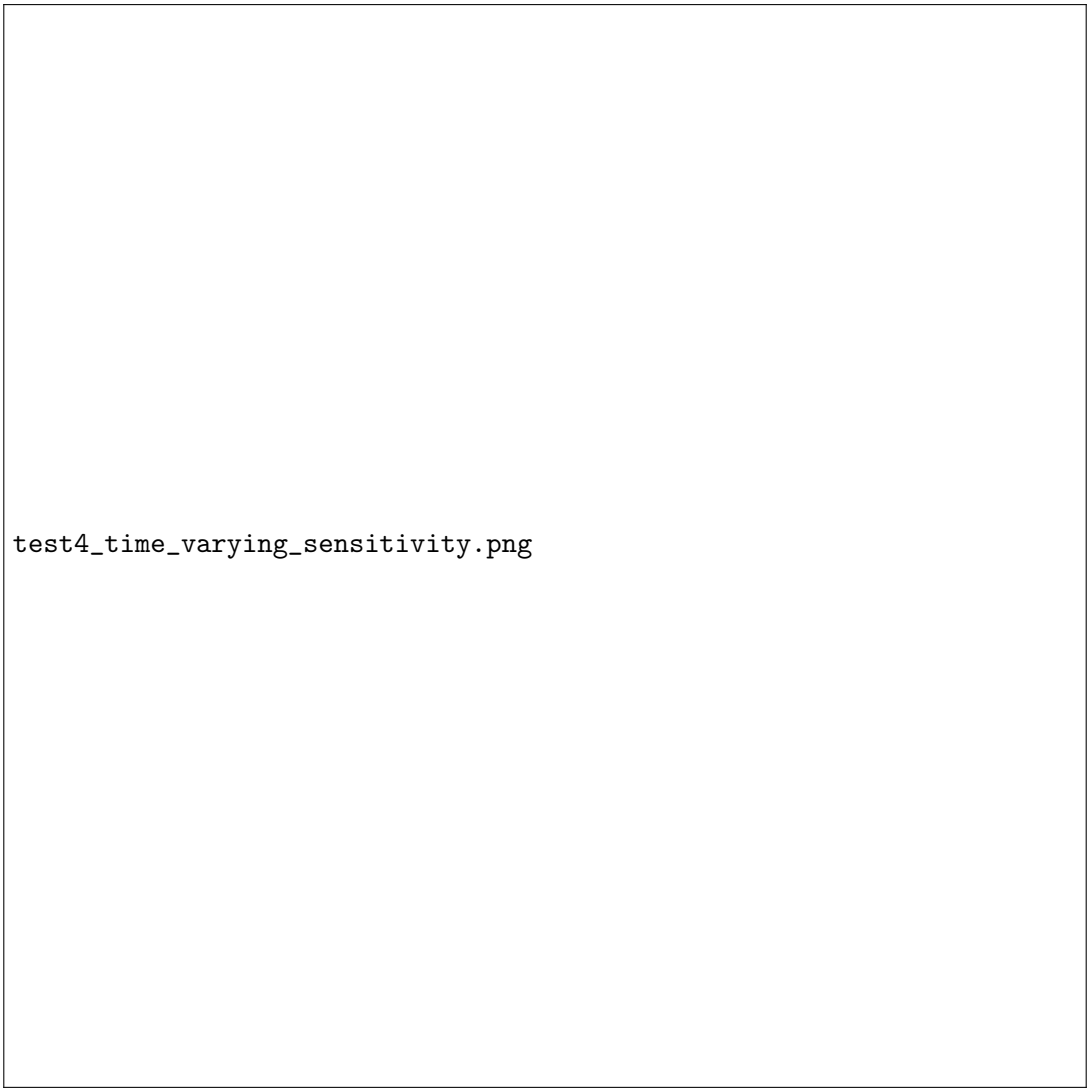

Figure 6: Time-varying sensitivity of the glucose dynamics $\dot{G}_p$ with respect to the most influential states along the baseline trajectory. Dominant states exhibit persistent influence across the entire postprandial horizon.

10.3 Cumulative Influence and Effective Dimensionality

Figure 7 shows the cumulative contribution of states to the total normalized output sensitivity, ordered from highest to lowest influence. The cumulative curve reaches approximately 95% of the total influence after the inclusion of only three states. Beyond this point, adding additional states yields negligible incremental contribution.

This result indicates that, from the perspective of the output map alone, the effective dimensionality of the glucose dynamics is extremely low. The dominant behavior of $\dot{G}_p$ can be captured by a small subset of states, with the remaining states contributing marginally under the tested operating regime.

10.4 State Ranking and Role Classification

Table 1 summarizes the ranked state influences, along with a qualitative classification of whether each state influences glucose dynamics directly or indirectly. Direct states correspond to those

Figure 7: Cumulative normalized influence of states on the glucose dynamics $\dot{G}_p$, ordered by decreasing sensitivity. The dashed line marks the 95% cumulative influence level.

appearing explicitly in the glucose balance equations, while indirect states affect glucose through intermediate pathways.

States whose mean sensitivities fall below the 1% relative threshold are identified as low-influence states. These include insulin mass compartments, gastric storage compartments, and auxiliary dynamics that do not directly shape the glucose rate equation under nominal conditions.

10.5 Interpretation and Implications

The results of Test IV demonstrate that the instantaneous glucose dynamics are governed by a very small subset of states, with the majority of the model states exerting negligible direct influence on $\dot{G}_p$ along the baseline trajectory. This finding is structurally consistent with the form of the glucose balance equations and complements the results of the previous diagnostics.

Importantly, classification as a low-influence state does not imply physiological irrelevance or dispensability in all contexts. Rather, it indicates that, under the tested regime and output

Table 1: Ranking of state influence on glucose dynamics based on mean absolute sensitivity of $\dot{G}_p$.

Rank	State	Mean Sensitivity	Role
1	G_t	7.90×10^{-2}	Direct
2	G_p	6.71×10^{-2}	Direct
3	I_{po}	6.18×10^{-2}	Indirect
4	I_d	9.00×10^{-3}	Indirect
5	Q_{gut}	6.58×10^{-4}	Indirect
6–12	remaining states	≈ 0	Indirect

restriction, such states do not materially shape the local evolution of plasma glucose. These results therefore provide output-map-level evidence that can be integrated with energy, time-scale, and identifiability analyses to inform principled reduced-order modeling decisions.

11 Synthesis of Diagnostic Results and Structural Implications

This section integrates the outcomes of the four diagnostic tests into a coherent structural interpretation of the nonlinear glucose–insulin model. The objective is not to introduce new analyses, but to reconcile the evidence obtained from complementary perspectives—input–output energy, time-scale structure, parameter identifiability, and output map sensitivity—into a unified picture. All conclusions are explicitly conditional on the operating regime, excitation design, and measurement restrictions stated earlier.

11.1 Convergence of Evidence Across Diagnostics

Although each test interrogates a distinct structural property of the model, a consistent pattern emerges when the results are viewed collectively.

Test I demonstrated that, under physiologically admissible excitation, the realized input–output energy is overwhelmingly concentrated in the gastrointestinal compartments, with all other states contributing negligibly to the joint controllability–observability metric. This indicates that, from an energy transmission perspective, upstream glucose appearance dynamics dominate the response of the measured output.

Test II revealed a pronounced and persistent separation of time scales across the postprandial trajectory. Fast relaxation modes on the order of minutes coexist with slow modes on the order of hours, with a separation ratio of approximately two orders of magnitude. The stability and consistency of this separation across early, peak, and recovery phases indicate that stiffness and fast–slow organization are intrinsic properties of the model dynamics rather than transient artifacts.

Test III showed that, even under deliberately excitation-rich and optimistic experimental conditions, the Fisher Information Matrix associated with glucose-only measurements remains severely ill-conditioned. The worsening of conditioning under richer excitation provides strong evidence that the loss of parameter identifiability is structural, arising from intrinsic confounding in the parameter-to-output map rather than from insufficient input design.

Test IV isolated the structure of the output map itself and demonstrated that the instantaneous glucose dynamics are governed by a very small subset of states. In particular, only

plasma and tissue glucose states exert persistent, dominant influence on $\dot{G}_p$, while the majority of states affect glucose only indirectly or negligibly along the baseline trajectory.

Taken together, these results converge on the conclusion that the effective input–output behavior of the model is both low-dimensional and strongly constrained by structural features that cannot be overcome by excitation alone.

11.2 Structural Redundancy and Slaving Relationships

The combination of strong time-scale separation (Test II) and sparse output sensitivity (Test IV) suggests the presence of slaving relationships among states. Fast modes rapidly equilibrate and constrain the evolution of slower dynamics, while many states evolve on manifolds that are effectively parameterized by a small number of dominant variables.

From this perspective, states that exhibit negligible empirical energy (Test I), long characteristic time scales (Test II), poor identifiability (Test III), and vanishing output sensitivity (Test IV) can be interpreted as structurally redundant with respect to glucose-only observation. Their trajectories are determined largely by upstream states and parameters, and they contribute little independent information to the measured output.

Importantly, this redundancy is not a modeling defect but a direct consequence of the physiological abstractions embedded in the model structure and the restriction to a single measured output.

11.3 Implications for Reduced-Order Modeling

The diagnostics collectively provide a principled foundation for reduced-order modeling, while simultaneously imposing clear limits on what reduction can achieve. The results indicate that substantial state reduction is feasible from an input–output reproduction standpoint, particularly when the goal is to capture glucose dynamics alone. However, the same results also indicate that parameter identifiability and internal state reconstruction cannot be guaranteed within such reduced representations.

Crucially, no single diagnostic justifies state elimination in isolation. Rather, candidates for reduction are identified through the intersection of multiple criteria: low input–output energy, weak or indirect output sensitivity, participation primarily in fast or slaved modes, and persistent non-identifiability under rich excitation. States satisfying all of these conditions are strong candidates for exclusion in reduced-order representations tailored to glucose-centric objectives.

11.4 Limits of Inference

All conclusions drawn in this section are conditional on the assumptions articulated earlier. In particular, they depend on the use of plasma glucose as the sole measured output, the normoglycemic operating regime, and the optimistic assumptions embedded in the excitation and noise modeling. The diagnostics do not rule out the possibility that additional measurements, alternative operating regimes, or fundamentally different experimental designs could alter the structural conclusions.

Accordingly, the synthesis presented here should be interpreted as a rigorous characterization of the model's structure under a specific but practically relevant observational constraint, rather than as a universal statement about the model in all contexts.

11.5 Role of the Diagnostics as Research Tools

Finally, it is important to emphasize that the four diagnostic tests employed in this work are not intended as standalone decision rules, but as complementary research tools. Their value lies in their collective ability to expose hidden structure, reveal intrinsic limitations, and prevent overconfident interpretation of numerical success.

In this sense, the diagnostics do not merely support reduced-order modeling decisions; they also clarify why certain goals—such as full parameter identifiability from glucose-only data—are fundamentally unattainable within the chosen framework. This clarity is itself a central scientific result of the present analysis.

12 Limitations, Assumptions, and Scope of Validity

This section explicitly delineates the assumptions under which the analyses in this document are valid, the limitations inherent to the adopted modeling and diagnostic framework, and the scope within which the resulting conclusions should be interpreted. No new results are introduced. All statements in this section are direct consequences of the model structure, the implemented code, and the four diagnostic tests presented earlier.

12.1 Restriction to Glucose-Only Measurement

All diagnostics performed in this work are conditional on plasma glucose being the sole measured output. Empirical input–output energy, Fisher Information analysis, and output map sensitivity are all formulated exclusively with respect to $G_p(t)$. No insulin measurements, tracer data, or auxiliary physiological outputs are incorporated.

As a consequence, all conclusions regarding state relevance, parameter identifiability, and redundancy are properties of the *input–output pair* consisting of the nonlinear model and glucose-only observation. They do not constitute statements about the intrinsic observability or identifiability of the full physiological system under richer measurement sets. Structural non-identifiability identified in this work is therefore output-induced rather than an inherent flaw of the underlying physiological representation.

12.2 Optimistic Noise and Modeling Assumptions

Where identifiability-related diagnostics are employed, the underlying assumptions correspond to an optimistic or best-case scenario. In particular, the empirical Fisher Information Matrix is constructed without explicit modeling of measurement noise correlations, sensor delays, saturation effects, or model mismatch. Implicitly, the analysis assumes homoscedastic, uncorrelated noise and a structurally correct model.

These assumptions are not intended to reflect realistic sensing conditions. Rather, they serve to establish an upper bound on achievable identifiability. Failure to identify parameters or resolve degeneracies under such optimistic assumptions implies that identifiability cannot be recovered under more realistic noise models or sensing limitations.

12.3 Structural Nature of Identifiability Limitations

The excitation-rich identifiability analysis demonstrates that increasing input richness amplifies dominant sensitivity directions while further suppressing weakly identifiable ones. The resulting deterioration of Fisher Information conditioning under designed excitation indicates that parameter confounding is structural in nature.

Accordingly, poor identifiability observed in this work cannot be attributed to insufficient excitation, short simulation horizons, or numerical artifacts. Instead, it arises from the algebraic and dynamical structure of the model when viewed through the glucose-only output map. This conclusion is strictly empirical but is supported consistently across all excitation scenarios tested.

12.4 Local and Trajectory-Dependent Time-Scale Analysis

Time-scale separation results are derived from local linearizations of the nonlinear dynamics along a nominal postprandial trajectory. Jacobian eigenvalues and associated time constants therefore characterize local relaxation behavior around specific operating points, rather than global properties of the state space.

Although the persistence of strong time-scale separation across multiple trajectory phases suggests robustness, no claim is made regarding global invariant manifolds or uniform time-scale separation under arbitrary initial conditions or inputs. The reported fast–slow structure should be interpreted as a property of the examined operating regime.

12.5 Output-Preserving Nature of Reduction Implications

Any implications for reduced-order modeling derived from the diagnostics are explicitly output-preserving in nature. The analyses identify states and parameters that are redundant with respect to reproducing plasma glucose dynamics, not with respect to maintaining full physiological interpretability or internal state fidelity.

As a result, reduced-order models informed by these diagnostics should be understood as effective input–output representations tailored to glucose dynamics. They are not intended to serve as complete physiological surrogates, nor to support reliable inference of internal insulin kinetics or parameter values without additional measurements.

12.6 Operating Regime and Physiological Scope

All simulations and diagnostics are conducted within a normoglycemic, postprandial operating regime. Certain physiological mechanisms, such as renal glucose excretion and extreme nonlinear threshold effects, are intentionally disabled or inactive within this regime.

Consequently, the conclusions presented here do not extend to pathological conditions such as severe hyperglycemia, hypoglycemia, or disease states in which additional regulatory mechanisms become dominant. Extension of the present analysis to such regimes would require revisiting both the model configuration and the diagnostic assumptions.

12.7 Summary of Scope

In summary, the results of this work provide a rigorous characterization of structural redundancy, time-scale separation, and identifiability limitations for a nonlinear glucose–insulin model

under glucose-only observation and optimistic experimental assumptions. Within this scope, the conclusions are strong and internally consistent. Outside this scope, no claims are made, and extrapolation is neither intended nor justified.

13 Conclusions and Outlook

This work has presented a systematic, multi-diagnostic analysis of a nonlinear glucose–insulin model with the explicit goal of characterizing structural relevance, time-scale organization, identifiability, and output dependence under glucose-only observation. Rather than relying on a single analytical lens, four complementary tests were employed, each probing a distinct aspect of the model's structure. The resulting conclusions are therefore not isolated findings, but the convergence of independent lines of evidence.

13.1 Summary of Principal Findings

The empirical input–output energy analysis demonstrated that, under physiologically admissible excitation, the effective transmission of inputs to the measured output is dominated by a small subset of states, primarily associated with glucose appearance dynamics. Many internal states, while physiologically meaningful, contribute negligibly to realized input–output energy in the examined regime.

The trajectory-based time-scale analysis revealed strong and persistent separation between fast and slow dynamical modes across multiple phases of the postprandial response. This separation indicates stiffness and slaving relationships that constrain the evolution of the system to a low-dimensional manifold over most of the trajectory.

The excitation-rich identifiability analysis showed that increasing input richness does not alleviate, and in fact exacerbates, ill-conditioning of the Fisher Information Matrix associated with glucose-only measurements. This result provides strong empirical evidence that parameter non-identifiability is structural rather than excitation-limited.

Finally, the output map sensitivity analysis demonstrated that the instantaneous glucose dynamics are governed directly by only a very small number of states, with the majority of states exerting only indirect or negligible influence on $\dot{G}_p$ along the nominal trajectory.

13.2 Integrated Interpretation

Taken together, these findings establish that the effective input–output behavior of the model is both low-dimensional and structurally constrained. Redundancy arises not from poor numerical conditioning or insufficient excitation, but from the intrinsic organization of the model when viewed through a single measured output. The same structural features that produce physiological realism at the state level also induce confounding and slaving that limit identifiability and internal state reconstruction.

Within this context, reduced-order representations are not merely computational conveniences but structurally justified abstractions. However, such reductions must be interpreted carefully: they preserve glucose dynamics by collapsing internally redundant mechanisms, not by faithfully reproducing all physiological processes.

13.3 Implications for Future Modeling and Experimentation

The results of this study clarify several directions for future work. From a modeling perspective, they suggest that efforts to estimate or interpret large parameter sets from glucose-only data are fundamentally ill-posed and should be avoided or reformulated. From an experimental perspective, they indicate that additional measurements, rather than additional excitation, are required to overcome structural identifiability limitations.

More broadly, the diagnostic framework employed here provides a template for rigorously interrogating complex physiological models before engaging in estimation, control, or reduction. By treating numerical degeneracy and failure as informative outcomes rather than errors, the framework helps prevent overconfident interpretation and guides principled model simplification.

13.4 Closing Remarks

This work emphasizes that understanding the limitations of a model is as important as demonstrating its capabilities. By explicitly identifying where information is lost, where dynamics are slaved, and where structure constrains inference, the analysis provides a transparent foundation for subsequent reduced-order modeling, control design, or experimental augmentation. Within its stated scope, the conclusions are robust; beyond that scope, they invite careful and deliberate extension rather than unwarranted extrapolation.

References

References

[1] E. Dalla Man, R. A. Rizza, and C. Cobelli, "Meal simulation model of the glucose–insulin system," *IEEE Transactions on Biomedical Engineering*, vol. 54, no. 10, pp. 1740–1749, 2007.